Information content of SNR/resolution trade-offs in three-dimensional magnetic resonance imaging

S. Portnoy,[a] S. C. Kale, and A. Feintuch
Mouse Imaging Centre, Toronto Centre for Phenogenomics, Toronto, Ontario M5T 3H7, Canada

C. Tardif and G. B. Pike
McConnell Brain Imaging Centre, Montreal Neurological Institute, Montreal, Quebec H3A 2B4, Canada

R. M. Henkelman
Mouse Imaging Centre, Toronto Centre for Phenogenomics, Toronto, Ontario M5T 3H7, Canada
and Department of Medical Biophysics, University of Toronto, Toronto, Ontario M5G 2M9, Canada

(Received 28 February 2008; revised 20 February 2009; accepted for publication 21 February 2009; published 30 March 2009)

In MRI, a trade-off exists between resolution and signal-to-noise ratio, since different fractions of the available scan time can be used to acquire data at higher spatial frequencies and to perform signal averaging. By comparing a wide variety of 3D isotropic MR scans with different combinations of SNR, resolution, and scan duration, the impact of this trade-off on the image information content was assessed. The information content of mouse brain, mouse whole-body, and human brain images was evaluated using a simple numerical approach, which sums the information contribution of each individual *k*-space data point. Results show that, with a fixed receiver bandwidth and field of view, the information content of trade-off images is always maximized when the SNR is equal to about 16. The optimal imaging resolution is dependent on the scan duration, as well as certain MR system properties, such as field strength and coil sensitivity. These properties are, however, easily accounted for with the acquisition of a single scout MR image, and the optimal imaging resolution can then be calculated using a simple mathematical relationship. If the imaging task is approached with a predetermined resolution requirement, the same scout scan can be used to calculate the scan duration that will provide the maximum possible information. Using these relationships to maximize the image information content is an excellent technique for guiding the initial selection of imaging parameters. © *2009 American Association of Physicists in Medicine*.
[DOI: 10.1118/1.3098124]

Key words: information content, MRI, SNR, resolution

I. INTRODUCTION

The time available for acquiring the data for a magnetic resonance image can be deployed in two quite different strategies. Since MR image quality is always limited by signal-to-noise ratio (SNR), time can be spent repetitively acquiring low resolution data to improve the SNR of the image. This results in excellent soft tissue discrimination but at limited resolution. Alternatively, image acquisition time can be deployed to acquire data at higher spatial frequencies (high order *k*-space) resulting in images with finer spatial resolution (smaller voxels) but restricted SNR. A compromise choice with respect to SNR and spatial resolution must be made for every MR image acquired. This choice is often dictated by convention or historical experience or standardized protocols. It is interesting therefore to attempt to understand this trade-off more formally in terms of the metric of image information.

The nonrecoverable trade-off between SNR and resolution is unique to MRI. In x-ray imaging, for instance, Poisson statistics dictate that the noise in any pixel is proportional to the square root of the signal.[1,2] As a result, any SNR loss incurred by reducing the pixel size can be fully recovered by binning adjacent pixels.[1–3] In MRI, the noise is constant and not related to the signal.[1] Therefore, rebinning will not fully compensate for the SNR loss that accompanies a resolution increase.

This fundamental difference implies that x-ray scans should be acquired with the finest possible pixel array and adjacent pixels can be averaged in the event that the resulting SNR is too low.[1,2] In MRI, however, it is necessary to approach an imaging task with *a priori* knowledge of the best compromise between resolution and SNR given the time available, since the consequences of an inappropriate choice cannot be fully compensated for retrospectively.

The objective of the current investigation is to determine how the trade-off between SNR and resolution affects the information content of MR images. The information content is a mathematical construct that was defined by Shannon over 50 years ago to predict the capacity of a communication channel.[4] More recently, it has been recognized that the radiologic image process can be viewed as a communication problem where an image source communicates with a receiver (or observer) via a channel.[5,6] Through the addition of noise and distortion, the channel (or imaging system) imposes fundamental limits on how much information can flow from the image source to the observer.[5] The information con-

tent has therefore been used to assess the performance of a variety of medical imaging systems, including CT,[6] x ray,[7,8] and MRI,[9–11] and medical image compression techniques.[12,13]

The information content was first applied to MR imaging by Fuderer in 1988,[9] who developed an expression for total image information I (in bits) in terms of the contrast to noise ratio (CNR) and resolution. Using this expression, Fuderer derived an approximate relationship between the optimal imaging resolution and the scan time. Several subsequent studies of MR image information content have calculated information using Fuderer's approach.[10,11,14] In the years following Fuderer's seminal paper, increases in magnetic field strength and progress in rf coil and gradient design have led to considerable improvements in image quality.[15,16] It is therefore useful to revisit the issue of information content using more state of the art, higher quality MR images, which allow for the statistical features of the data to be characterized more accurately.

In this paper, we evaluate the trade-off between SNR and resolution in terms of a calculated information metric. To do this, we begin with very high quality, isotropic volume MR data sets from three very different types of anatomy: Mouse brain, whole mouse body, and human brain. From these data, we show that the power spectrum of k-space data, $\bar{P}(k_r)$, follows the functional form

$$\bar{P}(k_r) = \alpha k_r^{-m} + P_N, \tag{1}$$

where $\bar{P}$ is the power spectrum integrated over a spherical shell of radius k_r and P_N is the power spectrum of the noise floor. What is most surprising is that the exponent m stays close to the value of 3 across the three very different looking images. Second, we show that the information content around the periphery of k-space is high. Third, we demonstrate that the integrated information content of both simulated and measured MR images appears to have a broad, shallow maximum over the trade-off between resolution and SNR, and that the peak corresponds to a particular SNR of about 16.

II. METHODS

II.A. High quality data acquisition

II.A.1. Mouse brain data

3D images of *in situ* fixed mouse brains were acquired on a 7T Varian Inova scanner (Varian Inc., Palo Alto, CA), using a fast spin echo (FSE) pulse sequence. Sequence parameters included TR=325 ms, ETL=6, ESP=8 ms, TE_{eff}=32 ms, FOV=14×14×25 mm^3, receiver bandwidth (BW) =149 kHz, and four averages. A total of ten mouse brain images were acquired using a single volume acquisition with matrix size 432×432×780 (producing 32 μm isotropic voxels). All data sets and simulated data correspond to three-dimensional isotropic resolution data. Each scan was 11.3 h long and three brains were imaged in parallel.[17] The average SNR of the acquired magnitude images was approximately 16. SNR values were calculated by dividing the mean of the signal over the entire object in a magnitude image by the standard deviation of the noise in an artifact-free background region. All SNR measurements reported in this study were obtained in this manner.

II.A.2. Mouse whole-body data

Using a spin echo sequence, a whole fixed mouse perfused with gadolinium was also imaged. Sequence parameters included TE/TR=19.15/600 ms, FOV=30×30×100 mm^3, BW=100 kHz, resolution=75 μm isotropic, and one average. The scan duration was 26 h and the SNR was 38.

II.A.3. Human brain data

A three-dimensional image of a postmortem human brain was acquired at 3 T using a spoiled gradient echo (SPGR) pulse sequence. Sequence parameters included TE/TR =5.65/23 ms, FOV=9×18×35 cm^3, BW=83 kHz, and 97 averages. The image resolution was 375×375×550 μm^3. The total imaging time was 64 h and the SNR was approximately 100.

II.B. Simulation of trade-off data

The collection of high quality MR images served as reference data sets, which were subsequently degraded to simulate images with shorter scan durations and different trade-offs between SNR and resolution. To generate the trade-off data, images with a range of isotropic voxel sizes (linear dimension d) were first created by truncating the acquired k-space data in all three directions (readout and both phase encodes). If d_{ref} is the linear dimension of the isotropic voxel in the reference image acquired with acquisition time T_{ref}, then the lowest resolution degraded image with pixel size d_{large} and no additional noise could have been acquired in a time T given by

$$T = \left(\frac{d_{ref}}{d_{large}}\right)^2 T_{ref}. \tag{2}$$

Other trade-off images at smaller pixel size (d) but with the same imaging time T could be simulated by adjusting the image noise to

$$\sigma = \sigma_{ref}\left(\frac{d_{ref}}{d_{large}}\right), \tag{3}$$

where σ_{ref} refers to the noise within the reference image or the reference raw data. Simple and well known relationships between σ and the image background standard deviation have been reported.[18] This adjustment requires addition of noise in quadrature to the acquired raw data equal to

$$\sigma_{added} = \sqrt{\sigma_{ref}^2\left(\frac{d_{large}}{d}\right) - \sigma_{ref}^2}. \tag{4}$$

There are a number of assumptions implicit in the trade-off described above. In particular, Eq. (2) assumes that the time saved by decreasing the image resolution results only from the decrease in the number of phase encode lines. With a

constant bandwidth, resolution reductions also decrease the readout time, but this does not reduce the overall scan time, since the repetition period, TR, was not changed accordingly. Changes in TR would lead to changes in image contrast, making the trade-off images noncomparable.

The noise added to trade-off images with voxel dimensions $d<d_{\text{large}}$ [see Eq. (4)] is related to the decrease in the number of averages required to reduce the voxel dimension without increasing the scan time. Decreasing the number of averages by a factor X increases the noise by $\sqrt{X}$.[19]

II.C. Calculating information content

The information content (in bits) of each three-dimensional trade-off image was calculated in k-space according to the equation provided by Fuderer:[9]

$$I=\frac{1}{2}\sum_{k_x}\sum_{k_y}\sum_{k_z}\log_2\frac{P_S(k_x,k_y,k_z)+P_N}{P_N}. \quad (5)$$

$P_S(k_x,k_y,k_z)$ refers to the signal power (i.e., square modulus of the signal) at spatial frequency position (k_x,k_y,k_z) and P_N refers to the noise power. The dependence of noise power on frequency is omitted, since the noise is assumed to be white. The above expression determines the information within the image by summing the individual contributions of each k-space data sample.

Information cannot be directly calculated in image space without taking into account the spatial correlation in intensity among image pixels. This correlation is significant and would be difficult to estimate. However, in k-space, one can make the reasonable assumption that k-space measurements are independent provided the object fills the field of view. Equation (5) therefore assumes that information is conserved between the spatial frequency and image domains. Since k-space and image space are equivalent representations of the same data, they should indeed contain equal information.

Before calculating information content using Eq. (5), there are a number of details to consider. The square modulus of the k-space signal, $|S(k_x,k_y,k_z)|^2$, can be seen as a measurement of P_S+P_N, since realistic data contain both signal and noise.[9] The P_N term in the numerator can therefore be omitted. In our case, however, the noise can be divided into two components: The physical and instrumental noise, which inherently exists in the acquired data (i.e., intrinsic noise σ_{ref}), and the noise that was added to k-space to simulate each trade-off (i.e., added noise σ_{added}). If P_S refers to the square modulus of the k-space data without added noise, then a term equal to the added noise power can still be included in both the numerator and the denominator. The intrinsic noise cannot, of course, be separated from the signal in this manner. Thus, a term for the intrinsic noise power is included in the denominator but not in the numerator. Equation (5) therefore can be evaluated as

$$I=\frac{1}{2}\sum_{k_x}\sum_{k_y}\sum_{k_z}\log_2\frac{|S(k_x,k_y,k_z)|^2+2\sigma_{\text{added}}^2}{2(\sigma_{\text{ref}}^2+\sigma_{\text{added}}^2)}, \quad (6)$$

where $|S(k_x,k_y,k_z)|^2$ refers to the square modulus of the original, undegraded k-space data at position (k_x,k_y,k_z). Noise powers are expressed in terms of their standard deviations, σ_{ref} and σ_{added}. For two independent Gaussian random variables (i.e., the real and imaginary noise components, n_I and n_Q) with zero mean and standard deviation σ, the mean power (i.e., $E[n_I^2+n_Q^2]$) is equal to $2\sigma^2$.

II.D. Acquisition of real trade-off data

To confirm the validity of the information calculations made from simulated trade-off data, experimental trade-off images of fixed mouse brain specimens were acquired with 21 and 11 min scan durations. For the 21 minute scan, images were acquired with isotropic resolutions of 90, 128, 156, and 180 μm and one, two, three, and four averages, respectively. For the 11 min scan, images with one, two, three, and four averages had isotropic resolutions of 125, 175, 218, and 250 μm, respectively. As with the simulated data, the bandwidth and field of view were kept constant at 110 kHz and $2.5\times1.4\times1.4$ cm^3. Three brains were scanned in parallel (in three individual coils),[17] resulting in a total of 24 trade-off images (3 brains $\times$ 4 trade-offs/scan duration $\times$ 2 scan durations).

By simulating most of the trade-off data, we obtained images with a broad range of SNR and resolution values by using arbitrary and fractional numbers of acquisitions (NEX). Achieving these trade-off data experimentally is much more difficult since only integral number of acquisitions can be used.

To accommodate experimental trade-off images with a broad SNR range, attenuators of varying strengths were placed in front of each of the three receiver channels (39 dB on channel 1, 36 dB on channel 2, and 30 dB on channel 3). With this attenuator configuration, the measured SNR values of the images were all between 7 and 135.

The information content of the acquired trade-off images was calculated using Eq. (6). Since no noise was added to these images, $\sigma_{\text{added}}=0$. σ_{ref} was equal to the standard deviation of the noise in the real and imaginary k-space components of the acquired trade-off data.

III. RESULTS

III.A. Spatial frequency power spectra

Spatial frequency power spectra, which plot the power of k-space data points against their distance, $k_r=\sqrt{k_x^2+k_y^2+k_z^2}$, from the center of k-space are plotted on a log-log graph in Fig. 1. The figure includes data for a single mouse brain image, the mouse whole-body image, and the human brain image. Representative image slices are shown at the right.

Rather than plotting each individual k-space data point, open circles at a given radius k_r represent the mean power of

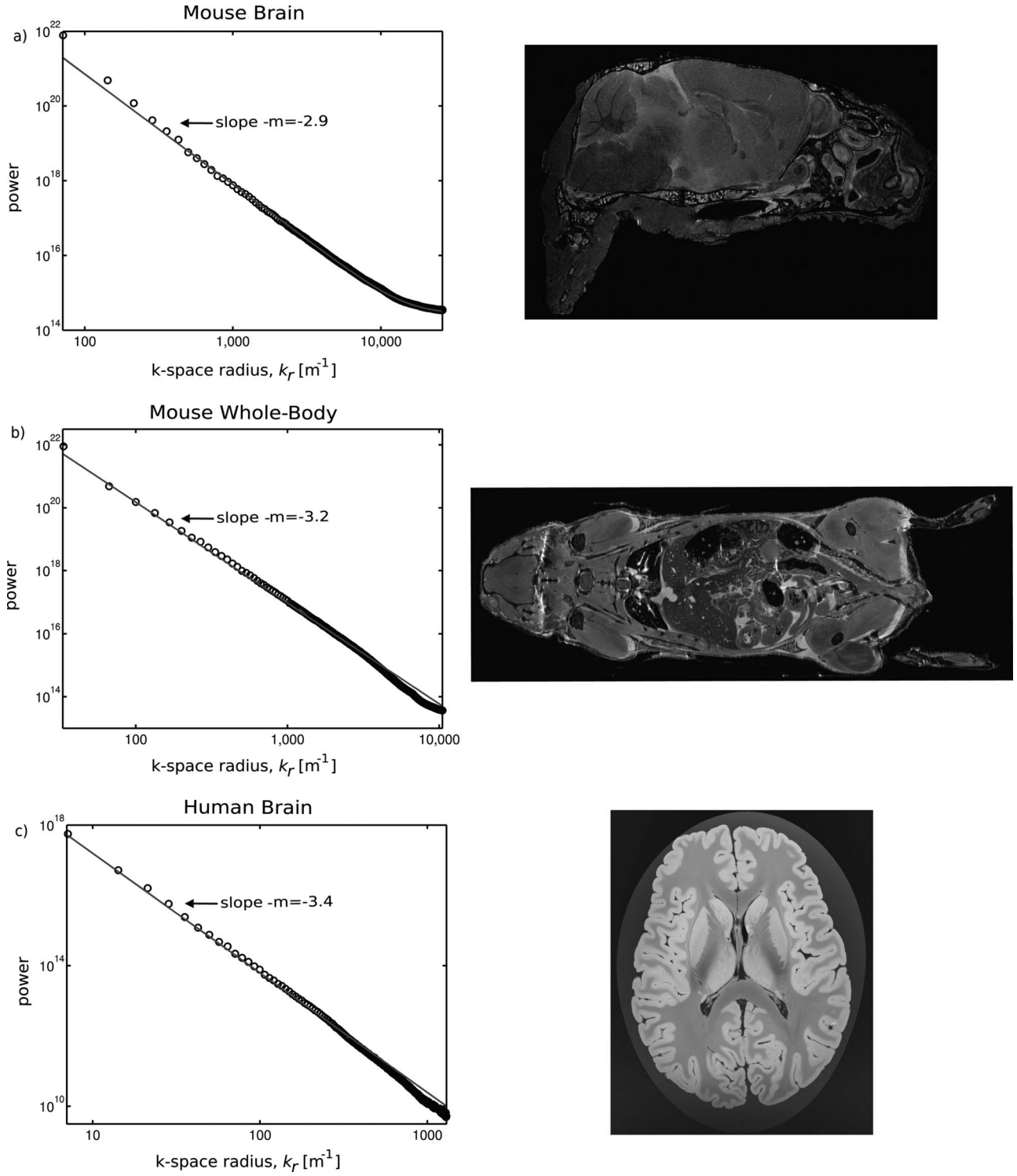

FIG. 1. Spatial frequency power spectrum for a reference (undegraded) mouse brain image (a), mouse whole-body image (b), and human brain image (c). A representative image from each of the three-dimensional data blocks is provided at the right side. Open circles represent the mean power of all points within a spherical shell in k-space. The shell thickness was equal to 71.4, 33.3, and 11.1 m^{-1} for the mouse brain, mouse whole-body, and human brain images, respectively. The solid lines represent a fit to a function of the form $\bar{P}(k_r)=ak_r^{-m}+P_N$.

all points within a spherical shell in k-space. The thickness of spherical shells was equal to the spacing between adjacent data points in the k_z direction ($\Delta k_z=1/\mathrm{FOV}_z$).

Over a broad range of spatial frequencies, all three of the spectra in Fig. 1 resemble a straight line on a log-log plot, indicating a power law decrease in signal power with k-space radius. The spectrum of the mouse brain image flattens at high spatial frequencies, as the noise power (noise floor) dominates over the signal. The mouse whole-body and human brain images have higher SNR values (38 and 100,

compared to 16 for the mouse brain). The noise floor is therefore further below the signal and the spectral flattening is less obvious.

Fitting the ten mouse brain data sets to a function of the form

$$\bar{P}(k_r) = ak_r^{-m} + P_N, \tag{7}$$

where P_N refers to the noise floor, yielded a decay constant, $m=2.87\pm0.07$. Fitting the mouse whole-body and human brain data sets yielded $m=3.2$ and $m=3.4$, respectively.

III.B. Information content of simulated trade-off images

Figure 2(a) shows representative slices obtained from five trade-off images generated from a mouse brain data set. The images have voxel dimensions ranging from 38 to 152 μm (increasing by factors of $\sqrt{2}$) and a simulated scan duration, T, of 21 min. Spatial frequency power spectra for these images are plotted in Fig. 2(b). The implications of the trade-off between SNR and resolution are visible in the power spectra: Spectra of higher resolution trade-offs extend further out in spatial frequency, but the noise floor is also more elevated, since the additional k-space extent was obtained at the expense of signal averaging.

The information spectra of the trade-off images, which plot the mean information within each spherical shell of k-space, $\bar{I}(k_r)$, are shown in Fig. 2(c). $\bar{I}(k_r)$ is calculated from $\bar{P}(k_r)$, the mean power per shell:

$$\bar{I}(k_r) = \frac{1}{2}\log_2\left[\frac{\bar{P}(k_r)}{2(\sigma_{\text{ref}}^2+\sigma_{\text{added}}^2)}\right]. \tag{8}$$

In the information spectra, the information content drops to zero at the noise floor. In addition, $\bar{I}(k_r)$ is higher in trade-off images with larger voxels. Since these lower resolution images have undergone more averaging, the noise power $(2\sigma_{\text{added}}^2)$ is reduced, which increases the information.

The total information per k-space radius can be estimated by multiplying the mean information, $\bar{I}(k_r)$, by the number of data points within each shell, $N_P(k_r)$, which is plotted in Fig. 2(d). As k_r increases, $N_P(k_r)$ initially increases quadratically, proportional to $4\pi k_r^2$. This continues until the outer diameter of the shell equals the width of the cubic 3D k-space data set (i.e., when $k_r\approx[2d]^{-1}$). After this point $N_P(k_r)$ decreases, as only a subset of points near the edges and corners of the k-space cube lies within subsequent shells.

The total information per k-space radius, $I(k_r)$, is plotted in Fig. 2(e). By integrating the total information per shell across all k-space radii, the overall information I is obtained. Of the trade-offs shown, the image with an SNR of 12.8 and a resolution of 54 μm (green) had the most information, as can be appreciated from Fig. 2(e).

The total information I within all the trade-off images generated from the mouse brain data set is plotted in Fig. 3. Figures 3(a) and 3(b) are plots of information content vs SNR and voxel size (d), respectively. Both plots include a family of seven curves, which correspond to different scan durations (0.7–42 min). Those data points that correspond to the trade-offs analyzed in Fig. 2 are marked by an "x." Two bars on each curve mark the boundaries between which the information content is within 95% of the maximum value.

Not surprisingly, as scan time increased so did information content. A doubling in scan time produced an ~1.5-fold increase in information. More surprising is the observation that for all scan durations, trade-offs with the maximum information had very similar SNR values. With an SNR of approximately 16 (dashed line), the information content never deviated from the maximum value by more than 5%. In contrast, the optimal resolution depended on the scan duration: As scan time increased, information was maximized at a finer resolution.

The data in Fig. 3 represent the observations obtained from just one of the ten mouse brains. The remaining nine data sets did, however, produce very similar results (see Fig. 4). Although there was some variation in the absolute information, the maximum information for each individual mouse brain image was always obtained at an SNR of 16, demonstrating that this finding is not dependent on the specifics of an individual image.

Plots of information content versus SNR for trade-off images generated from the mouse whole-body and human brain data sets are shown in Fig. 5. In spite of the visible differences in the character of these images, the results are remarkably similar. In particular, the information was once again maximized for SNR≈16, regardless of the simulated scan duration.

Although the SNR at which information is maximized is relatively constant, there is some jitter in the peak location [see Figs. 3(a) and 5]. However, in a theoretical simulation of the ideal case, where the signal and noise components of the image data could be perfectly separated, such that $P_S=\alpha k_r^{-3}$ and σ was exactly determined by Eq. (3), the peaks lined up perfectly at SNR≈16. This suggests that any peak movement is the result of experimental measurement and is not attributable to any real trend.

III.C. Information content of acquired trade-off images

The information content of the acquired trade-off images is plotted versus SNR in Fig. 6. There are three sets of data points (black, red, green) that correspond to trade-off images obtained from the three imaging coils, which were attenuated to different degrees.

In all cases, the four data points that correspond to a set of trade-off images acquired from a single coil with a single scan duration lie precisely along a curve. The shape of the curve is very similar to those plotted in Fig. 3(a) for the simulated mouse brain data. In fact, each solid line in Fig. 6 is a cubic-spline interpolation of the average curve in Fig. 3(a), which was not changed in shape but simply translated upward or downward to minimize the sum of square differences between it and the four trade-off data points.

As with the simulated data, trade-offs with SNR values closest to 16 had the most information. In addition, for all

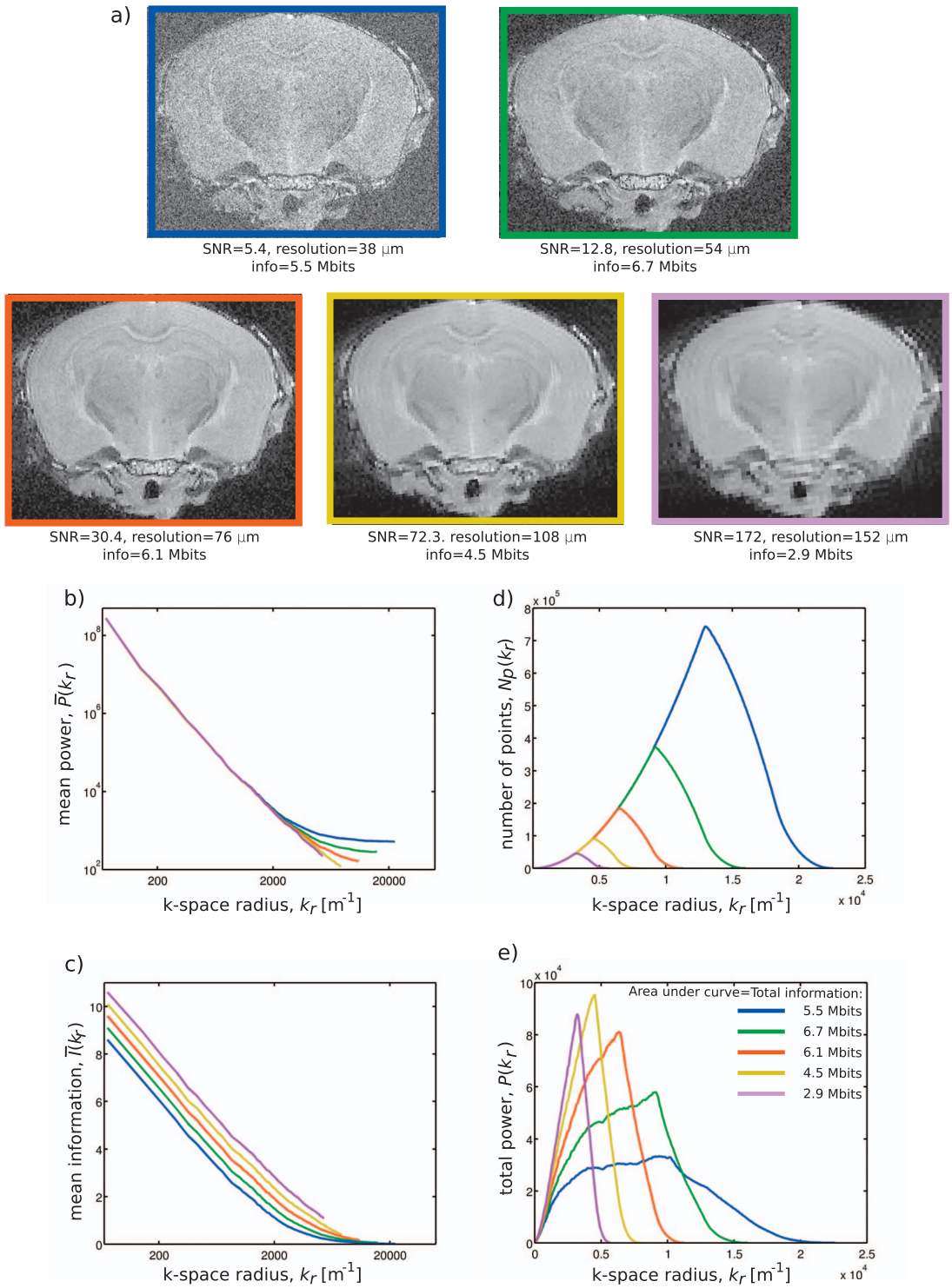

FIG. 2. Calculating information content. (a) A collection of five trade-off images generated from the mouse brain data, with a simulated scan duration, T, of 21 min (a representative slice is shown). (b) Spatial frequency power spectrum of each trade-off image. (c) Mean information per sample inside each spherical shell of k-space. (d) Number of data points within each shell. (e) Total information per shell. All plots are color coded according to the corresponding image.

three coils, a factor 1.5 increase in information was observed between the 11 and 21 min scan durations. The excellent agreement between the acquired and simulated data confirms the accuracy and validity of the simulated trade-off images.

IV. DISCUSSION

In this investigation, 3D MR images of mouse brain, mouse whole-body, and human brain specimens were used to study the effect of the SNR/resolution trade-off on the information content. As demonstrated in Fig. 1, the power spectra of these distinctive images were remarkably similar, all exhibiting power law behavior with a decay constant of approximately -3. This decay constant was also observed by Fuderer for a wide variety of human scans, including spine, cardiac, and knee images, as well as a whole-body image.[9] Power spectra with decay constants in the range of roughly

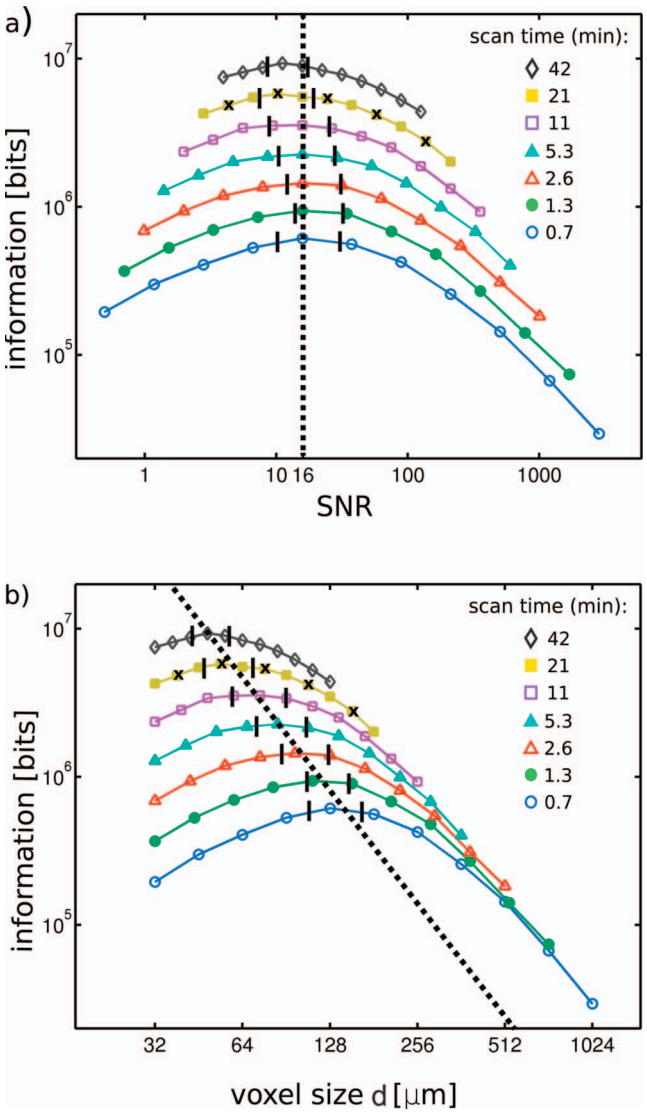

FIG. 3. Information content vs SNR (a) and resolution (b) for trade-off images generated from a single mouse brain data set. Those data points that correspond to the trade-off images analyzed in Fig. 2 are marked with an x. Vertical bars denote the band over which the information exceeds 95% of its maximum value.

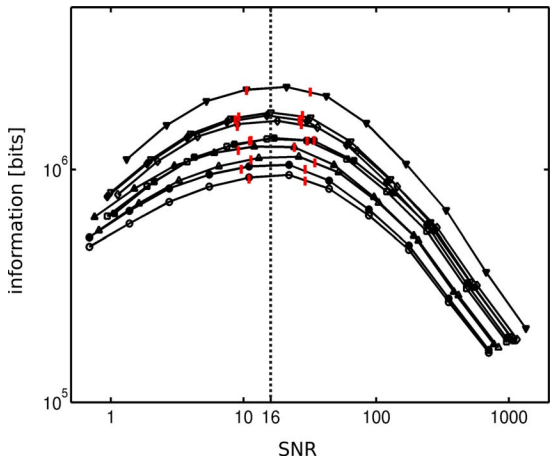

FIG. 4. Information content vs SNR for trade-off images generated from all ten mouse brain data sets (T=2.6 min). Vertical bars denote the band over which the information exceeds 95% of its maximum value.

-1.5 to -3 are typical of the entire subset of visual images known as "natural scenes."[20] The term natural scene broadly refers to images of the natural environment (e.g., landscapes, foliage, animals, etc). The power law behavior of these images is attributed to the property known as scale invariance, which assumes that statistical features of an image are independent of viewing distance.[21,22] It has also been attributed to the fractal nature of the images.[23]

Calculating the information content of the simulated and acquired trade-off images revealed that information was always maximized when SNR$\approx$16. Due to the similarity of their power spectra, this observation was true for the mouse brain, mouse whole-body, and even human brain data. It is therefore expected to be true of all anatomical MR images, which, as natural scenes, are known to have very similar spectral behavior.[9,20,21,24]

The observation that information is maximized at an SNR of only 16 should not be misinterpreted to imply that technical developments, such as increases in field strength and improvements in rf coil design, are unnecessary. Improvements to these aspects of the MR system are indeed welcome, since they make it possible to achieve an SNR of 16 at finer resolutions.

The effect of coil performance on the information content is seen in Fig. 6. Trade-off images obtained from coil 3, which was the least attenuated, had the highest absolute information. Furthermore, with the 21 min scan duration, the 90 μm trade-off image had the most information. In contrast, with coils 1 and 2, the maximum information was obtained at a resolution of 128 μm.

A more sensitive rf coil or higher field strength thus affects the information content in the same manner as an increase in scan time: The absolute information increases and the maximum occurs at a finer resolution. While the optimal SNR for maximum information is always equal to 16, the optimal voxel size is dependent on a variety of factors, including the scan duration and other system properties, such as field strength and coil performance. These properties can, however, be quite simply accounted for by acquiring a single baseline image with voxel dimension d_{baseline} and signal-to-noise ratio $\text{SNR}_{\text{baseline}}$. Assuming constant imaging time, bandwidth, and FOV, a factor X adjustment in resolution is accompanied by a factor $X^{5/2}$ change in SNR.[19] Therefore, the optimal voxel size d_{opt} can be calculated using the following relationship:

$$d_{\text{opt}} = d_{\text{baseline}} \left[\frac{16}{\text{SNR}_{\text{baseline}}} \right]^{2/5}. \quad (9)$$

Alternatively, if the imaging resolution has been predetermined based on the need to detect a feature of interest, the baseline image (with scan duration T_{baseline}) could be used to calculate the scan time T_{opt}, which would be necessary to obtain the maximum possible information:

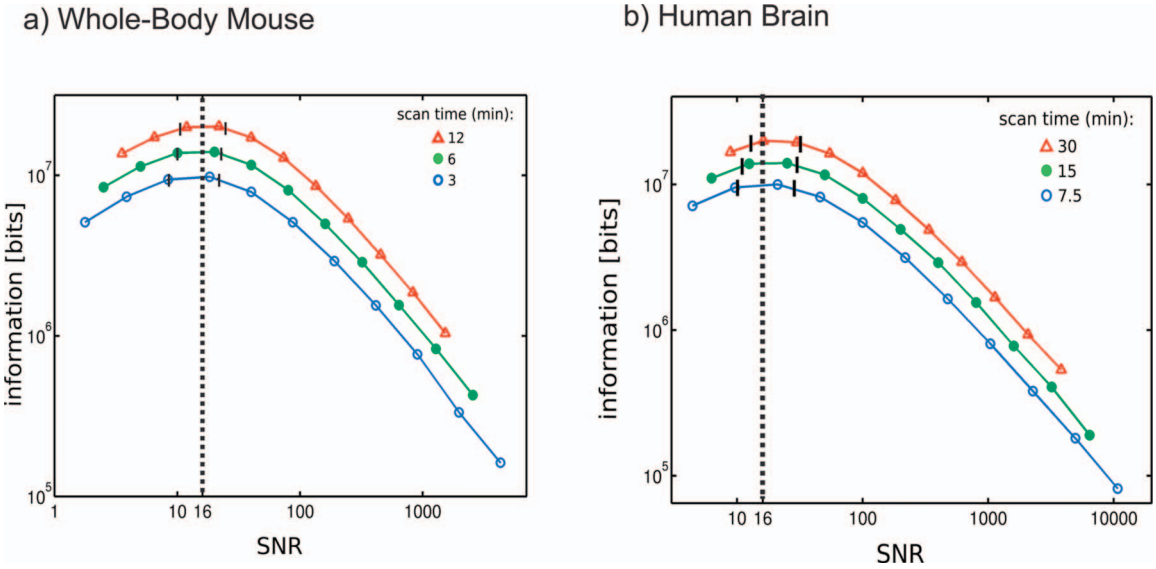

FIG. 5. Information content vs SNR for trade-off images generated from the mouse whole-body data (a) and for the human brain data (b). In all cases the maximum information content occurs at an SNR of 16.

$$T_{\text{opt}} = T_{\text{baseline}}\left[\frac{16}{\text{SNR}_{\text{baseline}}}\right]^2\left[\frac{d_{\text{baseline}}}{d_{\text{required}}}\right]^{5/2}. \quad (10)$$

Not all imaging tasks have an obvious resolution requirement. In mouse phenotyping by MRI screening (a particular interest of this laboratory), the size and scale of the abnormalities are often unknown. Therefore, there is no specific feature of interest that dictates the required resolution. In these cases, acquiring at the optimal imaging resolution, as determined by Eq. (9), can be helpful in ensuring good overall image quality. If, however, the necessary imaging resolution is known, it is appropriate to optimize the scan duration according to Eq. (10), since the benefits of high resolution will not be detectable if the scan is too short and the SNR is too low.[25]

The 95% boundaries indicated on the plots of information vs SNR and resolution (Figs. 3 and 5) are quite broad. In all cases, the upper bound of the 95% interval corresponded to at least a doubling in both SNR and voxel volume relative to the lower bound. The breadth of the information peak was also observed by Fuderer,[9] who described it as a convenient result, since small deviations from the optimal imaging resolution would not result in significant information losses. These substantial variations in SNR and resolution do, however, result in visible image quality differences [see, for example, Fig. 2(a)]. Therefore, images with very similar amounts of information may not be equally suited to a specific task. Striving to obtain more than 95% of the maximum possible information is a helpful starting point to guide the choice of imaging parameters; however, some additional optimization may be necessary to ensure that the resulting image is best suited for its ultimate purpose.[26,27]

A complete examination of the relationship between visual quality and information content is beyond the scope of this investigation. Some insight can, however, be gained from a qualitative examination of the images shown in Fig. 2(a). The information metric effectively ruled out the first (38 μm) trade-off image, which is far too noisy, and the last (152 μm) trade-off image, which is too pixelated. The image in the set with the most information (54 μm, 6.7 Mbits) may, however, be slightly too noisy to obtain the highest quality score in an observer preference study. A more likely choice would be the middle (76 μm) image. The observation that images optimized for information appeared slightly low in SNR was consistent throughout this study. While it is

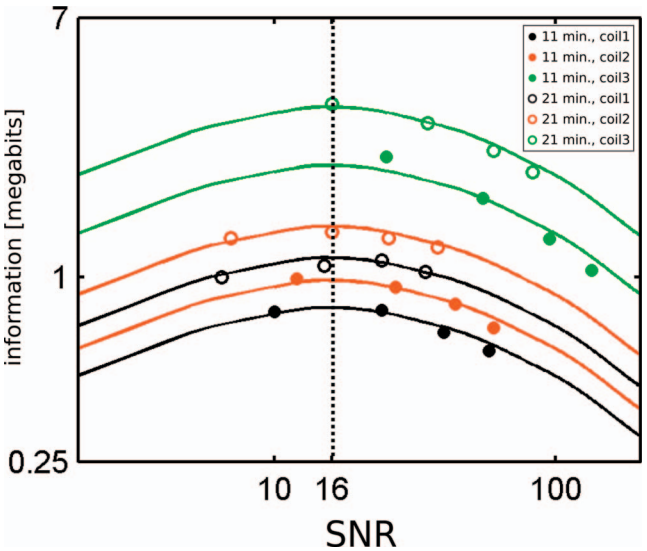

FIG. 6. Information content vs SNR for the acquired mouse brain trade-off images. Each solid line is a cubic-spline interpolation of an SNR versus information curve from Fig. 3(a) for 21 min or 11 min acquisitions, which was not changed in shape but simply translated upward or downward to minimize the sum of square differences between it and the four trade-off data points. This vertical shift corrects for variation in gain of the receiver chains and also for the additional hardware attenuations. All experimental points are consistent with the simulations and identify an SNR of 16 as optimal.

linked with the information content, the human perception of image quality is affected by a variety of other factors, which relate to the unique sensitivities of the human visual system.[28,29] It is therefore not surprising that human observers preferred additional SNR at the expense of resolution and a small loss of information.

In a recent study of the information content of MR thumb images, Saeed *et al.* showed a correlation between the information metric and the human perception of image quality.[10] Specifically, a monotonically increasing relationship was observed between image information and observer assigned quality scores. A plateau was, however, encountered, where increases in information content were no longer accompanied by significant increases in the quality score.

The high quality data used in this investigation provide a clear demonstration of the robust statistical features that, as natural scenes, all anatomical MR images share. It also motivated the decision to calculate information without using the equation provided by Fuderer that incorporates a contrast-to-noise ratio,[9] unlike other recent studies of MR image information content.[10,11] Fuderer's equation is based on the assumption that the power spectra of MR images behave according to the function

$$P(k_r) = a\left(k_r^2 + \left(\frac{\varepsilon}{2\pi}\right)^2\right)^{-3/2}. \quad (11)$$

In accordance with our observations, the above expression indicates that the decay of signal power is proportional to k_r^{-3} for large k_r. However, within the expression, Fuderer includes an additional parameter, ε, which characterizes a flattening of the spectrum at low spatial frequencies. While a plateau at small k_r values was a property of the images used by Fuderer (which has been attributed to having a field of view larger than the object[20]), this was not observed in the high quality data used in this investigation. As such, a fit of Eq. (11) to the power spectra of our images yielded ε values of less than 0.01. This conflicts with Fuderer's assumption that ε is significantly larger than unity, which he used to incorporate the CNR into the expression for information content.[9] The information within our trade-off images was therefore calculated using Eq. (6), which simply sums the information of each individual *k*-space data point and makes no model assumptions about the structure of the power spectrum.

Along with the finding that information peaks when SNR $\approx$ 16, this investigation provides insight into the distribution of image information within the spatial frequency domain. It is no surprise that, as shown in the information spectra of Fig. 2(c), a single data point near the center of *k*-space has more information than a single point near the edge. The spread of information throughout *k*-space is, however, the result of a compromise between the quantity and quality of data points. Much of the information therefore lies further out in *k*-space, where there are more data points. This is seen in the plots of total information per *k*-space shell [Fig. 2(e)], where the two highest resolution trade-off images (38 and 54 μm) have a peak in information at $k_r \approx 10\,000\ \mathrm{m}^{-1}$. The remaining trade-off images were too low in resolution to reach this point, and their information peaks coincided with the maximum in the number of data points per shell.

At $k_r = 10\,000\ \mathrm{m}^{-1}$, the signal power has decayed by over 99% relative to the center of *k*-space and is dominated by the noise floor. While it may seem that the acquisition of data which are so dominated by noise is an inefficient use of scan time, the cumulative information content of these abundant data points exceeds that of the center of *k*-space. The contribution of noise dominated data points far from $k_r = 0$ to overall image quality was similarly noted by Watts and Wang, in their study investigating the noise limitation of detectable spatial resolution.[25]

V. CONCLUSION

In this study, we have investigated the use of an image information metric to inform the choice of using imaging acquisition time for improved SNR or increased spatial resolution in three-dimensional isotropic MR images. We have shown for several different types of anatomy that the power spectrum of the *k*-space data is linear on a log-log plot with an approximately invariant slope of -3 independent of the type of anatomy. We have also shown a method for calculating information and have demonstrated that the total information within a spherical shell in *k*-space increases with the radius of the shell, until boundaries are reached beyond which data should not be acquired. When optimized for maximum total information in a three-dimensional image, we have shown that the trade-off between SNR and resolution will be decided in terms of an image SNR of approximately 16. While this serves as only an approximate guideline for image acquisition planning, the analysis has provided insight into the structure of acquired MR anatomical data and the relative information contributions of various parts of *k*-space to MR images.

[a]Author to whom correspondence should be addressed. Electronic mail: sportnoy@phenogenomics.ca; Telephone: (647)-837-5811; Fax: (647)-837-5832.

[1]W. A. Edelstein *et al.*, "The intrinsic signal-to-noise ratio in NMR imaging," Magn. Reson. Med. **3**, 604–618 (1986).
[2]D. Parker and G. Gullberg, "Signal-to-noise efficiency in magnetic resonance imaging," Med. Phys. **17**, 250–257 (1990).
[3]R. T. Constable and R. M. Henkelman, "Contrast, resolution, and detectability in MR imaging," J. Comput. Assist. Tomogr. **15**, 297–303 (1991).
[4]C. E. Shannon, "Communication in the presence of noise," Proc. IEEE **86**, 447–457 (1998).
[5]H. R. Sheikh, A. C. Bovik, and G. de Veciana, "An information fidelity criterion for image quality assessment using natural scene statistics," IEEE Trans. Image Process. **14**, 2117 (2005).
[6]R. F. Wagner, D. G. Brown, and M. S. Pastel, "Application of information theory to the assessment of computed tomography," Med. Phys. **6**, 83–94 (1979).
[7]I. Brodie and R. Gutcheck, "radiographic information theory and application to mammography," Med. Phys. **9**, 79–95 (1982).
[8]H. Kanamori and M. Matsumoto, "The information spectrum as a measure of radiographic image quality and system performance," Phys. Med. Biol. **29**, 303–313 (1984).
[9]M. Fuderer, "The information content of MR images," IEEE Trans. Med. Imaging **7**, 368–380 (1988).
[10]T. M. Saeed, I. R. Summers, and W. Vennart, "Information content and quality of MR thumb images," Phys. Med. Biol. **48**, 3775–3785 (2003).

[11]X. Dongxiang *et al.*, "Information theoretic analysis of plaque in MR imaging," Proceedings of the IEEE International Conference on Image Processing **1**, 633–636 (2000).
[12]H. R. Sheikh and A. C. Bovik, "Image information and visual quality," IEEE Trans. Image Process. **15**, 430–444 (2006).
[13]R. M. Slone *et al.*, "Assessment of visually lossless irreversible image compression: Comparison of three methods by using an image-comparison workstation," Radiology **215**, 543–553 (2000).
[14]J. Bilbao *et al.*, "*K*-space information map," Proceedings of the International Society for Magnetic Resonance in Medicine Twelfth Scientific Meeting **12**, 2354 (2004).
[15]J. M. Tyszka, S. E. Fraser, and R. E. Jacobs, "Magnetic resonance microscopy: Recent advances and applications," Curr. Opin. Biotechnol. **16**, 93–99 (2005).
[16]T. W. Redpath, "Signal-to-noise ratio in MRI," Br. J. Radiol. **71**, 704–707 (1998).
[17]R. M. Henkelman *et al.*, "High throughput microimaging of the mouse brain," Proceedings of the International Society for Magnetic Resonance in Medicine Fourteenth Scientific Meeting **14**, 2010 (2006).
[18]R. M. Henkelman, "Measurement of signal intensities in the presence of noise in MR images," Med. Phys. **12**(2), 232–233 (1985); "Erratum: 'Measurement of signal intensities in the presence of noise in MR images,'" **13**(4), 544 (1986).
[19]A. Macovski, "Noise in MRI," Magn. Reson. Med. **36**, 494–497 (1996).
[20]R. M. Balboa, C. W. Tyles, and N. M. Grzywacz, "Occlusions contribute to scaling in natural images," Vision Res. **41**, 955–964 (2001).
[21]G. J. Burton and I. R. Moorhead, "Color and spatial structure in natural scenes," J. Opt. Soc. Am. B **26**, 157–170 (1987).
[22]E. P. Simoncelli and B. A. Olshausen, "Natural image statistics and neural representation," Annu. Rev. Neurosci. **24**, 1193–1216 (2001).
[23]D. J. Field, "relations between the statistics of natural images and the response properties of cortical cells," J. Opt. Soc. Am. A **4**, 2379–2394 (1987).
[24]R. Behin, J. Bishop, and R. M. Henkelman, ""Dynamic range requirements for MRI," Concepts Magn. Reson., Part B **26B**, 28–35 (2005).
[25]R. Watts and Y. Wang, "*K*-space interpretation of the Rose Model: Noise limitation on the detectable resolution in MRI," Magn. Reson. Med. **48**, 550–554 (2002).
[26]S. C. Kale *et al.*, "Optimization of the SNR-resolution tradeoff for registration of magnetic resonance images," Hum. Brain Mapp. **29**, 1147–1158 (2008).
[27]S. C. Kale *et al.*, "Trading off SNR and resolution in MR images," NMR Biomed. (in press).
[28]A. J. Maeder, "The image importance approach to human vision based image quality characterization," Pattern Recogn. Lett. **26**, 347–354 (2005).
[29]B. E. Rogowitz, T. N. Pappas, and J. P. Allebach, "Human vision and electronic imaging," J. Electron. Imaging **10**, 10–19 (2001).